Atmospheric
Chemistry
and Physics

Supplement of

Effects of the sample matrix on the photobleaching and photodegradation of toluene-derived secondary organic aerosol compounds

Alexandra L. Klodt et al.

Correspondence to: Rachel E. O'Brien (reobrien@umich.edu) and Sergey A. Nizkorodov (nizkorod@uci.edu)

Contents

Summary of Experiments Conducted

Table S1. Summary of the experiments carried out as part of this study at the College of William and Mary (WM) and the University of California Irvine (UCI).

Experiment Description	Data sets collected	Location
SOA preparation (x14)	Online-AMS	UCI
Trial experiments on aging of SOA in the aqueous phase (x5)	UV-Vis, LC-ESI-MS	UCI
Trial experiments on aging of SOA on filters (x2)	UV-Vis, Direct infusion ESI-MS, FTIR	WM
Aging of SOA in water and in 1 M ammonium sulfate (x3)	UV-Vis, LC-ESI-MS	UCI
Aging of SOA in water and on filter (x4)	UV-Vis, LC-ESI-MS, offline-AMS	UCI

Chamber OH Steady-State Estimation

The OH steady-state concentration in the chamber was estimated from the rate of depletion of the VOC reactant, in this case toluene. The rate of change of toluene concentration is given by Eq. S1.

$$\frac{d[VOC]}{dt} = -k_{OH}[OH]_{SS}[VOC] + k_{wall} \tag{S1}$$

Where $[VOC]$ is the concentration of toluene. $\frac{d[VOC]}{dt}$ is the change in toluene concentration with time, k_{OH} = 5.63 × 10^{-12} cm^3 molecule^{-1} s^{-1} (Calvert et al., 2002) is the bimolecular rate constant for the reaction of toluene with the OH radical, $[OH]_{SS}$ is the steady-state OH radical concentration, and k_{wall} is the loss rate due to uptake into the change wall and leaks, which is a minor process under our conditions. The gas-phase concentration of toluene, monitored by the ^{13}C isotope [^{13}CC$_6$H$_8$ + H]$^+$, was measured here using a Proton Transfer Time of Flight Mass Spectrometer (PTR-ToF-MS; Ionicon model 8000, Innsbruck, Austria), shown in Fig. S1(a). Integrating Eq. S1 and incorporating these values, we determined the OH steady-state concentration from Fig. S1(b) to be about 6 × 10^6 molecules cm^{-3}.
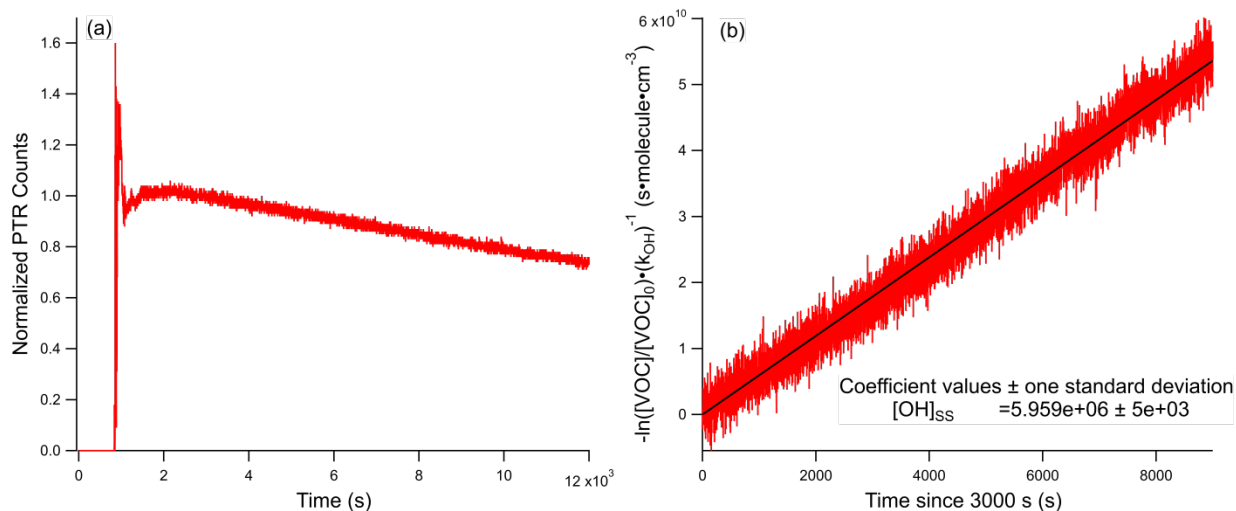
Figure S1. PTR-ToF-MS data (^{13}CC$_6$H$_8$ + H trace) used to estimate the OH steady-state concentrations in the chamber during SOA formation. The unsteady signal at early times arises from incomplete mixing in the chamber during the toluene injection. Panel (a) shows the data series normalized to the count value at 3000 s where we began the linear fit in panel (b). Panel (b) shows $-\ln\left(\frac{[VOC]}{[VOC]_0}\right) \times k_{OH}^{-1}$, with $\frac{[VOC]}{[VOC]_0}$ being the normalized PTR counts shown in panel (a), as a function of time since 3000 s as a rearrangement of Eq. S1. The slope of this trace represents the OH steady-state concentration in the chamber.

Scaling Photodegradation Rates to Atmospheric Conditions

The effective rate of photodegradation of SOA is given by Eq. S2.

$$J = \int F(\lambda)\phi(\lambda)\sigma(\lambda)d\lambda \qquad\qquad (S2)$$

Where $F(\lambda)$ is the spectral photon flux density, $\phi(\lambda)$ is the quantum yield for dissociation, and $\sigma(\lambda)$ is the effective Naperian (i.e., base e) absorption cross-section of the SOA. To calculate the predicted relative photodegradation rate in the atmosphere, we assumed the dissociation quantum yield was constant over the UV region (280 to 400 nm) and that the absorption cross-section of the SOA could be expressed as the measured mass absorption coefficient (MAC) scaled by a wavelength-independent constant. The relative rate of photodegradation in the atmosphere then simplifies to Eq. S3.

$$\frac{J_{atmosphere}}{J_{lamp}} = \frac{\int F_{atmosphere}(\lambda)MAC(\lambda)d\lambda}{\int F_{lamp}(\lambda)MAC(\lambda)d\lambda} \qquad\qquad (S3)$$

The spectral photon flux density ($F(\lambda)$) and the product ($F(\lambda) \times MAC(\lambda)$) for our photolysis set-up, the 24 h average values for LA (taken on June 20th), and the maximal achievable flux at the SZA = 0 are shown in Figure S2, and the ratios of theoretical atmospheric photodegradation rate to photodegradation rate in our set-up are shown in Table S2 The parameters used for the "Quick TUV" calculator (ACOM: Quick TUV, 2019) which was used to estimate the spectral flux densities were:

- Latitude/Longitude: 34°N 118°W or SZA = 0
- Date and Time: June 20, 2021
- Overhead Ozone: 300 du
- Surface Albedo: 0.1
- Ground Altitude: 0 km
- Measured Altitude: 0 km
- Clouds Optical Depth/Base/Top: 0.00/4.00/5.00
- Aerosols Optical Depth/S-S Albedo/Alpha: 0.235/0.990/1.000
- Sunlight Direct Beam/Diffuse Down/Diffuse Up: 1.0/1.0/0.0
- 4 streams transfer model.
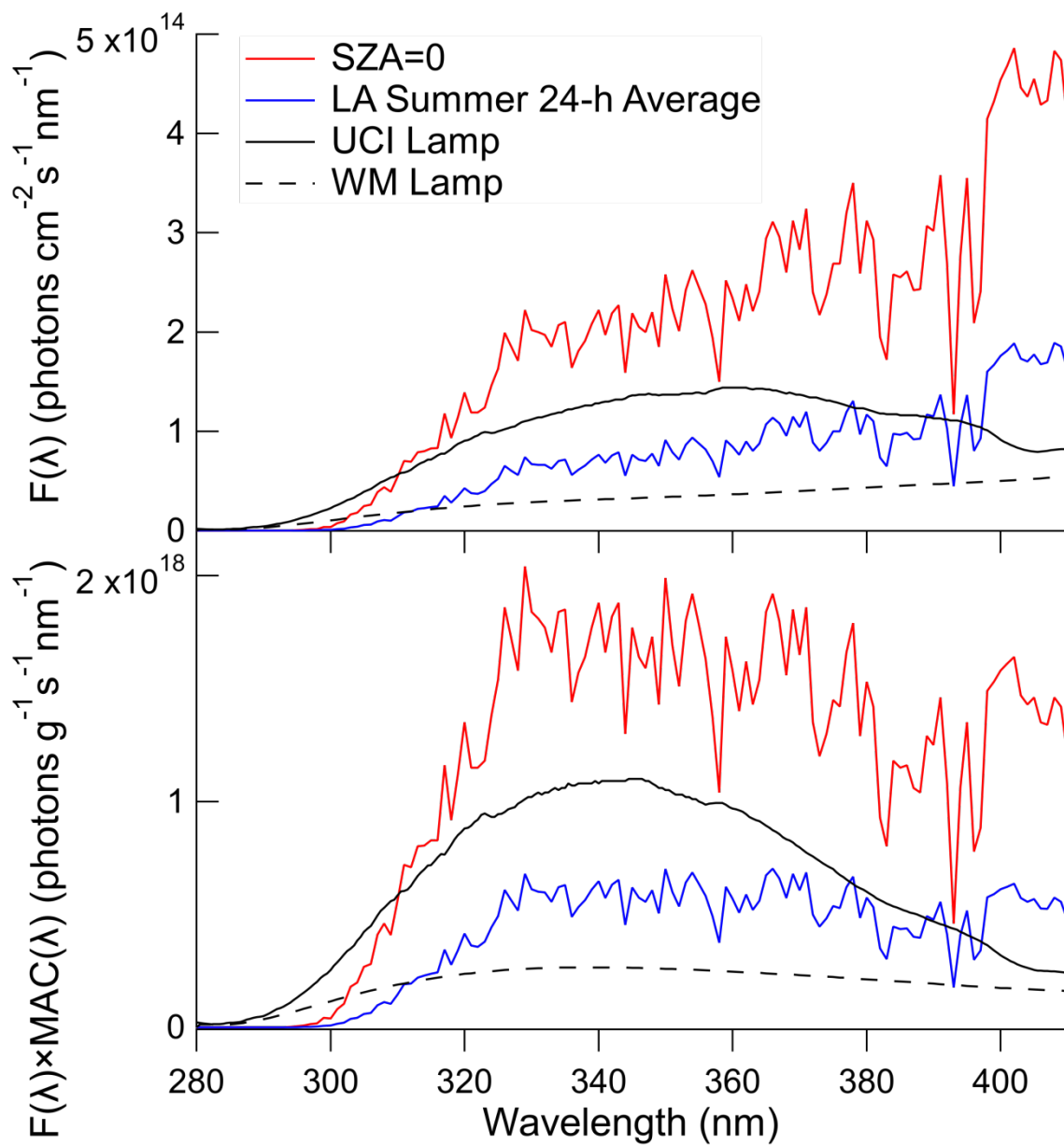
Figure S2. Spectral photon flux density ($F(\lambda)$) and its product with the mass absorption coefficient ($F(\lambda) \times MAC(\lambda)$) for UCI photolysis lamp (black solid), WM photolysis lamp (black dashed), solar zenith angle zero (red), and the Los Angeles 24-h average (blue).

Table S2. The integrated photon flux densities and the number of hours equivalent to one hour under our photolysis set-up for the 24-h average solar flux in Los Angeles in summer and the maximal achievable flux at the SZA = 0. The calculation was performed by integrating $F(\lambda) \times MAC(\lambda)$ from Figure S2 from 280 to 400 nm, the UV wavelength range that likely drives photochemistry for our samples. The values on the last two columns represent the ratios of the UV lamp's integrated flux to the solar integrated flux.

Lamp	Integrated $F(\lambda) \times MAC(\lambda)$ from the UV lamp (photons g⁻¹ s⁻¹)	Integrated $F(\lambda) \times MAC(\lambda)$ at SZA=0 (photons g⁻¹ s⁻¹)	Integrated $F(\lambda) \times MAC(\lambda)$ from the 24-h average in Los Angeles (photons g⁻¹ s⁻¹)	Equivalent hours at SZA=0	Equivalent hours at 24-h average sunlight in LA
UCI	7.94E19	1.32E20	4.62E19	0.6	1.7
WM	2.35E19	1.32E20	4.62E19	0.2	0.5

Aqueous Aging Summary

Table S3. Summary of aqueous SOA samples and their mass concentrations for aqueous-phase photolysis experiments. Mass concentrations from the same filter vary slightly between experiments aged in water versus aged in ammonium sulfate because the exact mass of the filter half was divided by the total mass of the filter and then multiplied by the mass of SOA collected in an attempt to account for differences in sizes of the filter sections. The mass concentrations are still somewhat approximate because the SOA may not have been completely evenly distributed on the filter after collection.

Photolysis experiment	Filter Number	Mass concentration for photolysis (mg L^{-1})
Water 1	4	233
Water 2	5	220
Water 3	6	238
Ammonium Sulfate 1	4	224
Ammonium Sulfate 2	5	249
Ammonium Sulfate 3	6	253

Extraction Efficiency Determination

After the initial extraction of the filter with 5 mL of acetonitrile, the filter was re-extracted in 3 mL of methanol and a UV-Vis spectrum was taken, showing the SOA extraction efficiency by acetonitrile from the filter was 90% or greater (the first UV-Vis spectrum was taken while the SOA was dissolved in 3 mL of water, so this should be an approximately equivalent comparison). SOA recovery from the ammonium sulfate solution was also tested. After the SOA was extracted from the evaporated solution of SOA in ammonium sulfate, 1 mL of water was added back to the residual salt, replacing the 1 mL of water which had been removed by rotary evaporation, and a UV-Vis spectrum was taken. Comparison of the post-extraction spectrum with the initial spectrum show that the extraction procedure generally recovered about 50-70% of the SOA from the ammonium sulfate solution. Results of a similar procedure with the samples which did not contain ammonium sulfate showed that more than 90% of the SOA was extracted if ammonium sulfate was not present. The reason for the retention of some 30-50% SOA by the wet ammonium sulfate residue is unclear and will be investigated in the future.
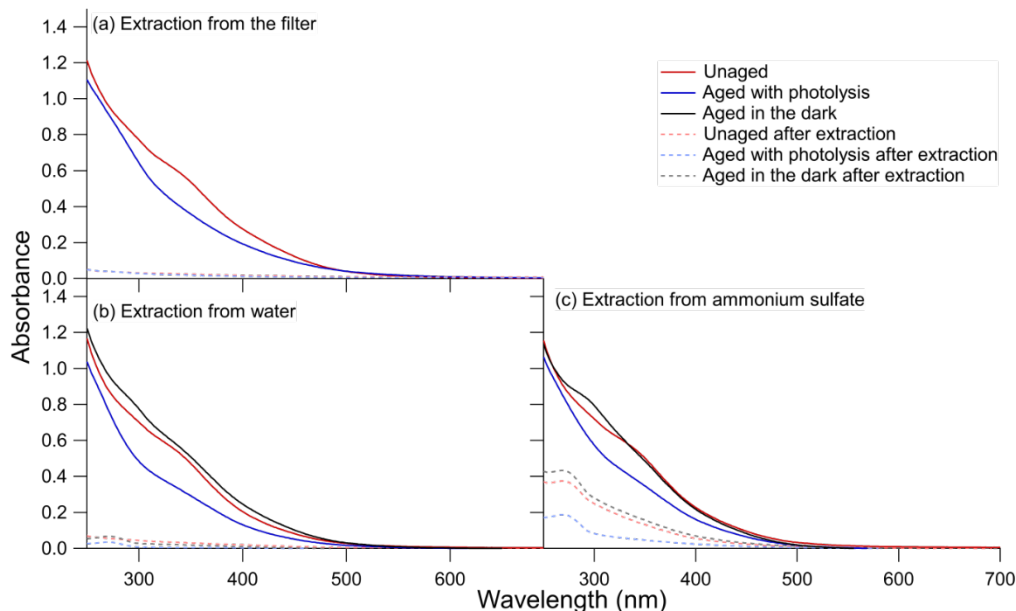
Figure S3. A test of the extraction efficiency of the toluene SOA (a) from the Teflon filters, (b) from the pure water solutions, and (c) from the 1 M ammonium sulfate solutions. After filters were initially extracted in acetonitrile, the filters were then submerged in 3 mL of methanol and shaken (but not stirred) for 10 minutes to extract any remaining SOA. Assuming that the integrated absorbance between 250 nm and 550 nm can be used as a metric for the amount of extracted SOA, >90% of the SOA was extracted from the filters. Recovery efficiency from the water and ammonium sulfate experiments was determined by adding 1 mL of water back to vial the SOA was extracted from, replacing the 1 mL of water which had been removed by rotary evaporation after SOA was extracted as described in the main text. Panel (b) shows that >90% of the SOA was recovered in the pure water conditions, but only 50 to 70% of the SOA could be recovered from the ammonium sulfate conditions in panel (c).

8

Supplemental Methods

WM Sample Preparation and Irradiation

The first set of on-filter photolysis experiments were carried out at the WM. Samples were irradiated in a photolysis box that has been described previously (Walhout et al., 2019). Briefly, the filter was sliced into four segments and three of the segments were placed in the box mounted vertically in front of a Xenon arc lamp (Newport model 66902). The photolysis box was air-tight, had a Teflon film (0.001 in inch) taped across a hole cut into the front panel to allow the UV radiation pass through, and had ~1-2 L min^{-1} of zero air (Environics 7000) at 50-60% RH continuously flowing through it. The spectral flux density on the irradiated filters is shown in Fig. S2. A second dark box was placed after the photolysis box with the same air flow. The control filter segment was placed there immediately, the second filter segment was moved there after 6 h of photolysis, the third filter segment was moved there after 18 h, and the irradiation ended after 24 h. This ensured that all the filter segments were exposed to the same air flow for the same amount of time, resulting in comparable SOA material loss to vaporization. The observed differences should therefore be dominantly due to photolysis, although we cannot fully rule out additional volatilization due to absorption of light by the chromophores in the SOA material.

Online AMS

The time series for the organic and nitrate were generated and this data is available online at the Index of Chamber Atmospheric Research in the United States (ICARUS) (Klodt, 2022). The same AMS as used for offline work was operated in V-mode (gen-alt) as opposed to fast mode which was used for the offline analysis discussed int eh main text. All other analysis was the same as described in the main text (Section 2.3.4).

UV-Vis Data
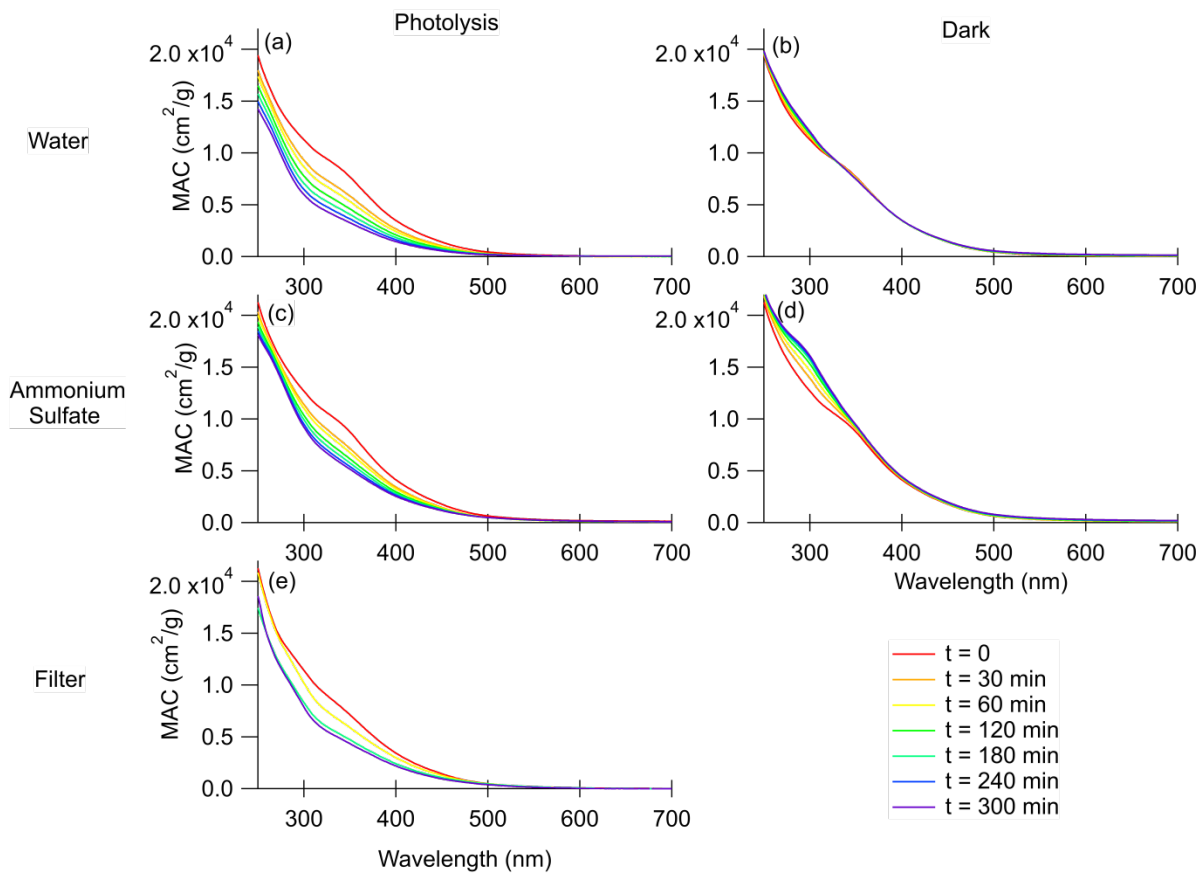
Figure S4. The wavelength-dependent mass absorption coefficient plots for each experimental condition and control. Photolysis in water is in panel (a), dark aging in water is in panel (b), photolysis in 1 M ammonium sulfate is in panel (c), dark aging in 1 M ammonium sulfate is in panel (d), and photolysis on the filter is in panel (e). Note that there are only four traces for the filter photolysis in panel e) because measuring the absorbance requires extraction of the filter and therefore is destructive.

Kinetic Measurements
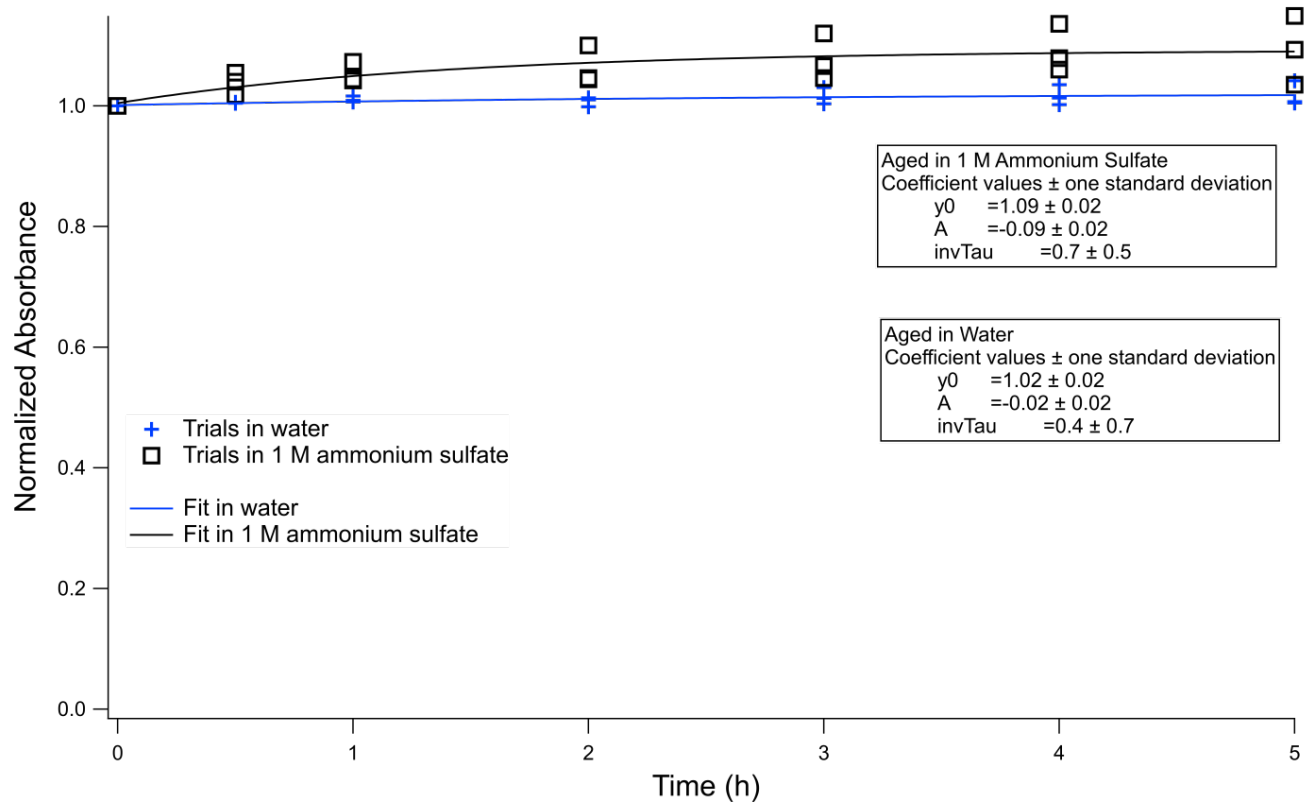
Figure S5. Changes in the normalized absorbance of wavelengths integrated from 300 to 700 nm in the dark for aqueous samples. Individual trials aged in water are shown with blue crosses and individuals trials aged in 1 M ammonium sulfate are shown with black squares. Fits are shown in blue for water and black form 1 M ammonium sulfate. The slight increase in absorbance in the ammonium sulfate solutions is due to reactions of ammonia with SOA carbonyl compounds producing light-absorbing products.
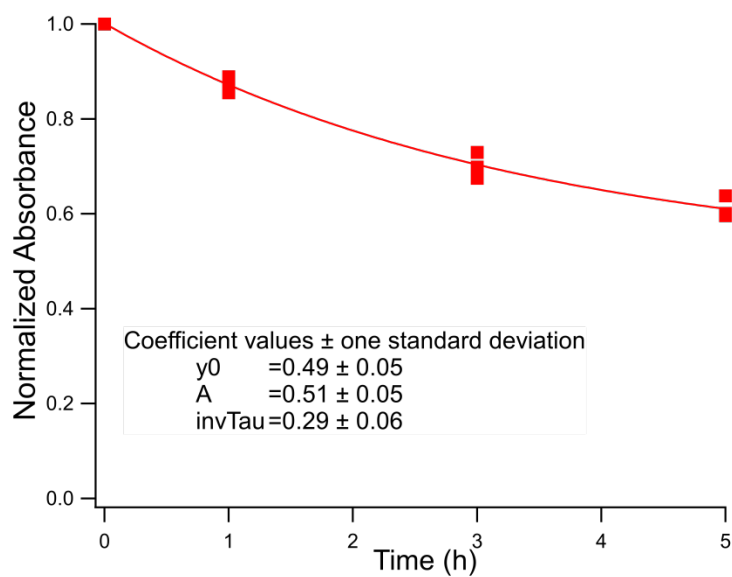
Figure S6. Normalized absorbance decay of wavelengths integrated from 300 to 700 nm with photolysis on the filter fit to a single exponential decay without constraining absorbance at time infinity to zero, i.e. allowing a photorecalcitrant fraction.

Table S4. Kinetic parameters for exponential and biexponential fits to absorbance data. Error represents the standard deviation of fitting parameters over the three combined trials.

	A_1	k_1 (h^{-1})	A_2	k_2 (h^{-1})
H_2O	0.79 ± 0.02	0.135 ± 0.007	0.21 ± 0.02	3.7 ± 1.0
AS	0.82 ± 0.04	0.08 ± 0.01	0.18 ± 0.04	3.1 ± 1.7
Filter	NA	NA	0.98 ± 0.01	0.102 ± 0.006

12
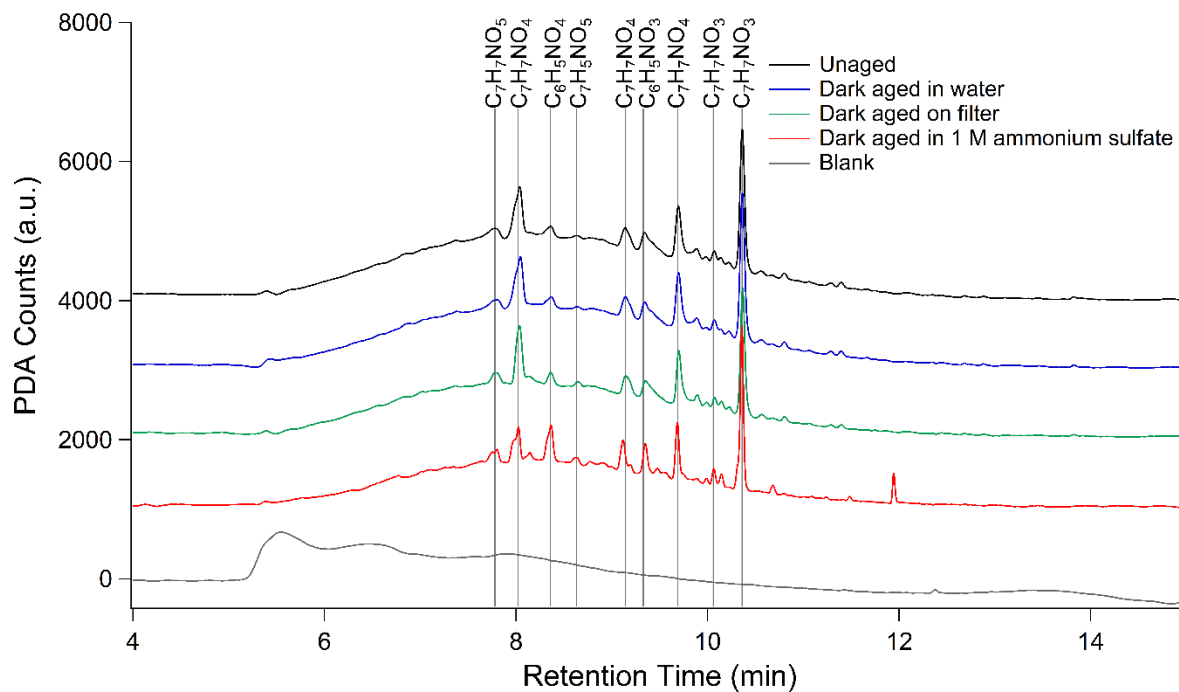
Figure S7. HPLC-PDA chromatograms for all dark conditions studied. PDA counts were integrated over 300 to 680 nm wavelength range. The blank PDA chromatogram shown as the last trace was subtracted from the rest of the traces. For display purposes, the traces are offset by adding 1000 unit spacing between them.

Table S5. Formulas associated with the well-defined peaks in the integrated (300 to 680 nm) unaged PDA data and the percent change from unaged after aging for individual peaks, the total resolved peak area, and the area of the unresolved baseline. The area of the unresolved baseline feature was calculated by integrating the sample PDA from 300 to 680 nm and summing from 5 to 12 min and then subtracting the area of the blank integrated from 300 to 680 nm summed from 5 to 12 min and the area of the resolved peaks.

PDA Retention Time (min)	Neutral Formula	Dark aged in Water – Filter 3 (% change)	Photolyzed in Water – Filter 3 (% change)	Dark aged on Filter – Filter 3 (% change)	Photolyzed on Filter – Filter 3 (% change)	Dark aged in Water – Filter 4 (% change)	Photolyzed in Water – Filter 4 (% change)	Dark aged in 1 M ammonium sulfate – Filter 4 (% change)	Photolyzed in 1 M ammonium sulfate - Filter 4 (% change)
7.78	$C_7H_7NO_5$	-18	-93	-13	-60	12	-30	40	-27
8.02	$C_7H_7NO_4$	-1	-32	-11	-95	5	-24	-9	-32
8.37	$C_6H_5NO_4$	-19	-36	-5	-92	8	-33	-5	-25
8.63	$C_7H_5NO_5$	-47	43	4	-88	-21	-74	-29	-43
9.14	$C_7H_7NO_4$	-1	-70	-12	-86	3	-67	-13	-71
9.33	$C_6H_5NO_3$	-7	-44	-9	-95	10	-49	0	-47
9.72	$C_7H_7NO_4$	8	-69	3	-84	10	-27	9	-15
10.06	$C_7H_7NO_3$	22	-92	-13	-100	-24	-99	-12	-100
10.35	$C_7H_7NO_3$	12	-29	-9	-95	15	-32	-19	-40
Total area 5 to 12 min (minus blank area)		**7**	**-35**	**-4**	**-29**	**9**	**-35**	**-19**	**-44**
Defined peak area		**2**	**-44**	**-8**	**-90**	**9**	**-37**	**-2**	**-37**
Unresolved baseline feature area		**8**	**-34**	**-3**	**-21**	**9**	**-35**	**-21**	**-45**

High Resolution Mass Spectrometry Results
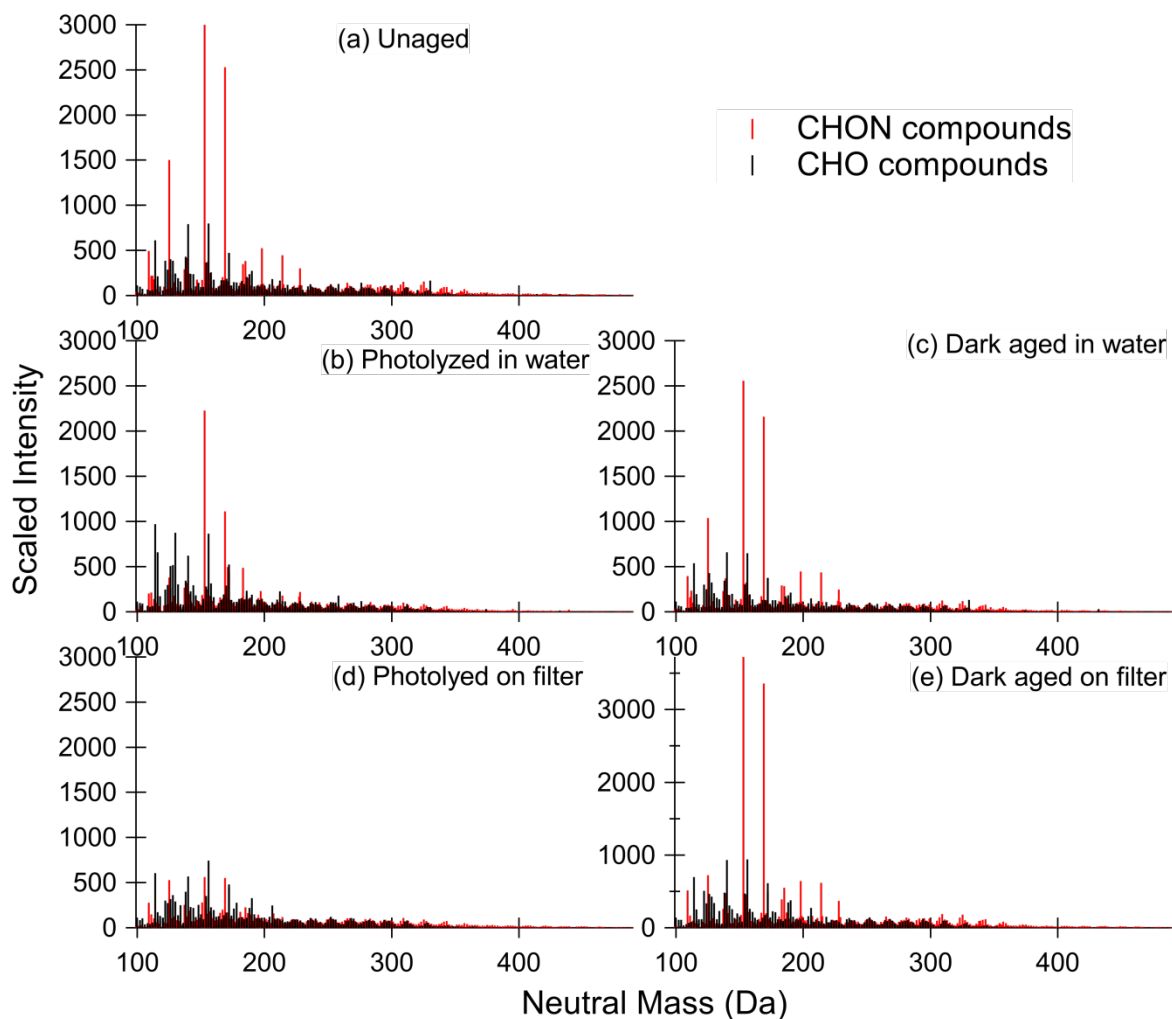
Figure S8. Mass spectra for all photolysis and dark aged samples comparing aging in water and on the filter. CHON compounds are shown in red and CHO compounds are shown in black. The three left panels are the same as in Figure 4 in the text, and the right panels show mass spectra for dark aging, which are not much different from the mass spectra for the unaged SOA.
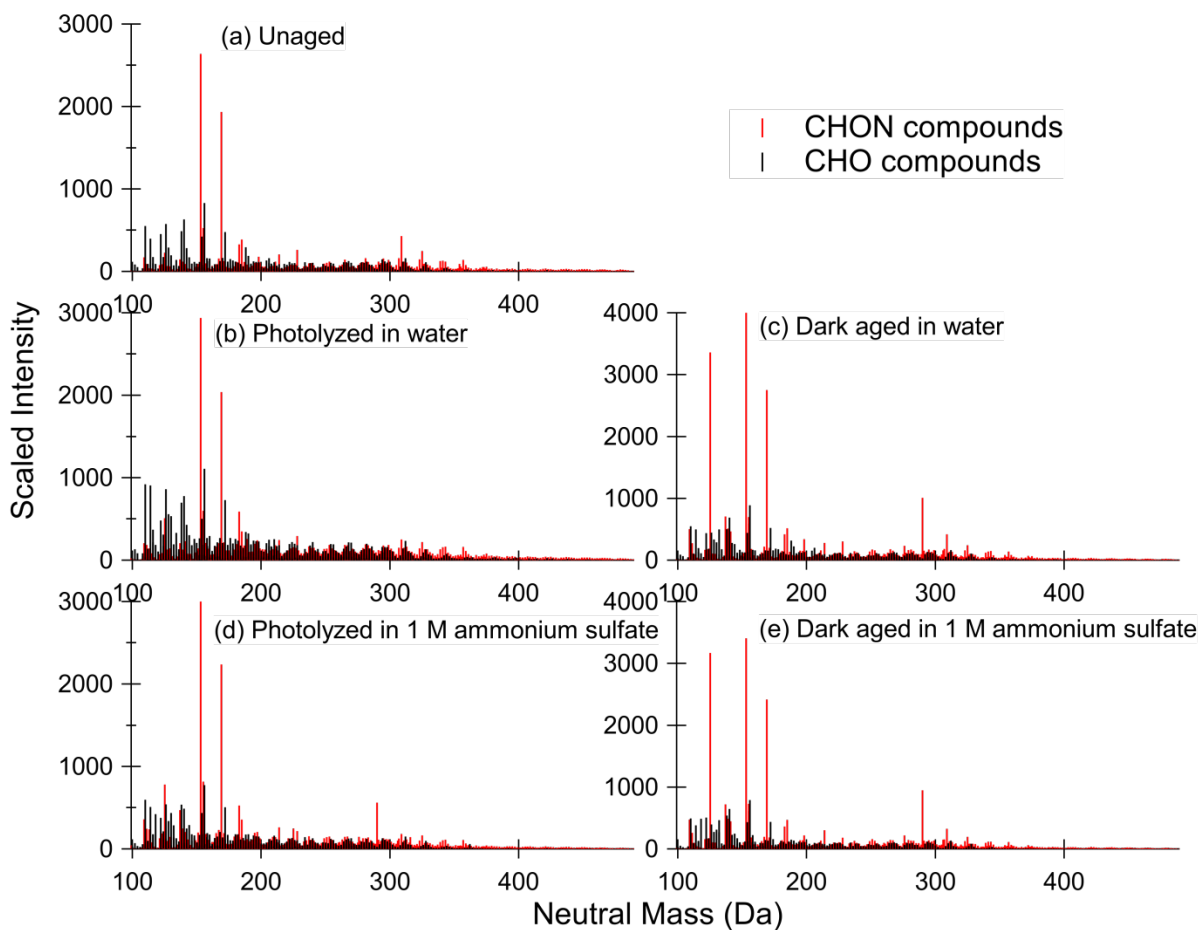
Figure S9. Mass spectra for all photolysis and dark aged samples comparing aging in water and 1 M ammonium sulfate. CHON compounds are shown in red and CHO compounds are shown in black. The three left panels are the same as in Figure 5 in the text, and the right panels show mass spectra for dark aging, which are not much different from the unaged SOA mass spectra.

Van Krevelen Diagrams
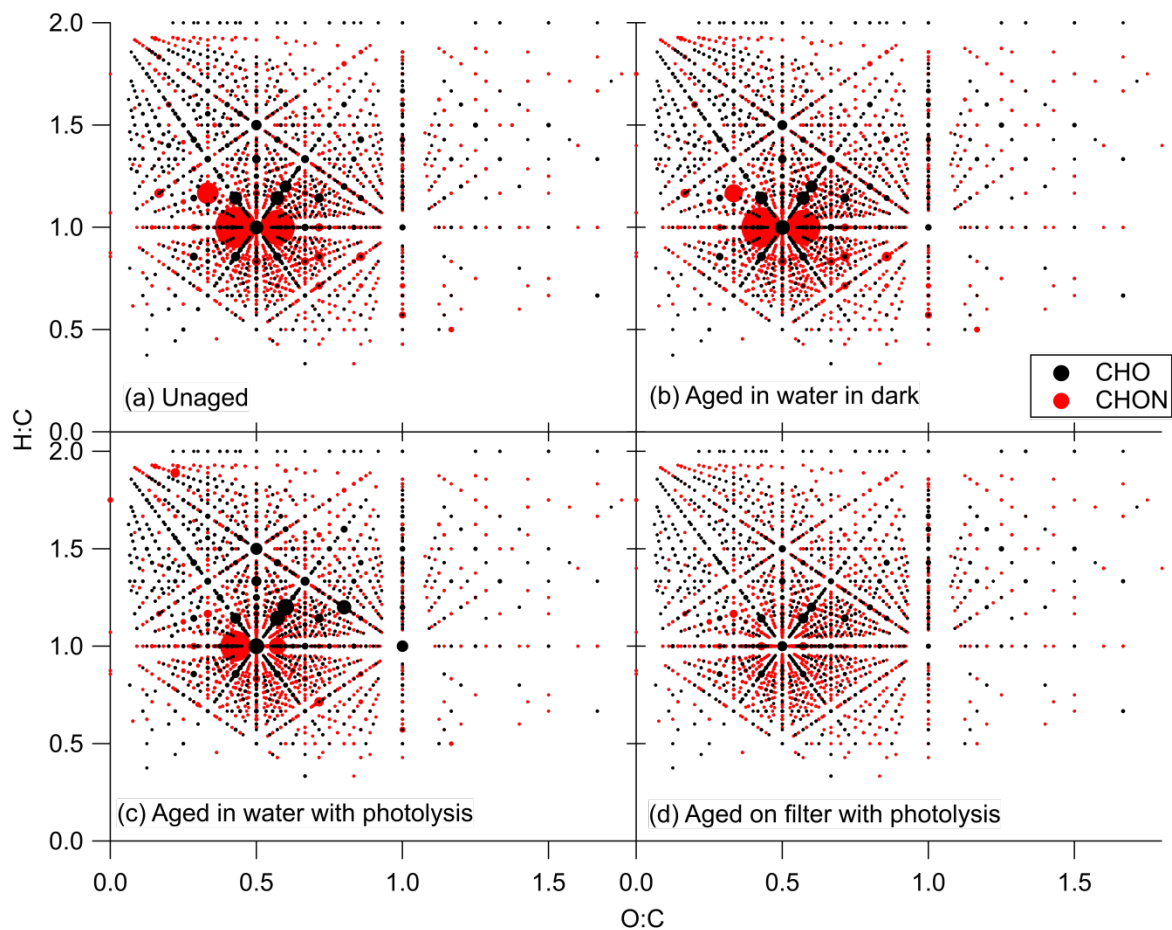
Figure S10. Van Krevelen diagrams for the (a) unaged sample, (b) sample aged in water in the dark, (c) sample photolyzed in water, and (d) sample photolyzed on the filter from Filter 3. CHO formulas are shown in black and CHON formulas are shown in red. The size of the marker represents the summed mass spectrometry abundance of all CHO or CHON compounds with the corresponding H:C and O:C ratios.
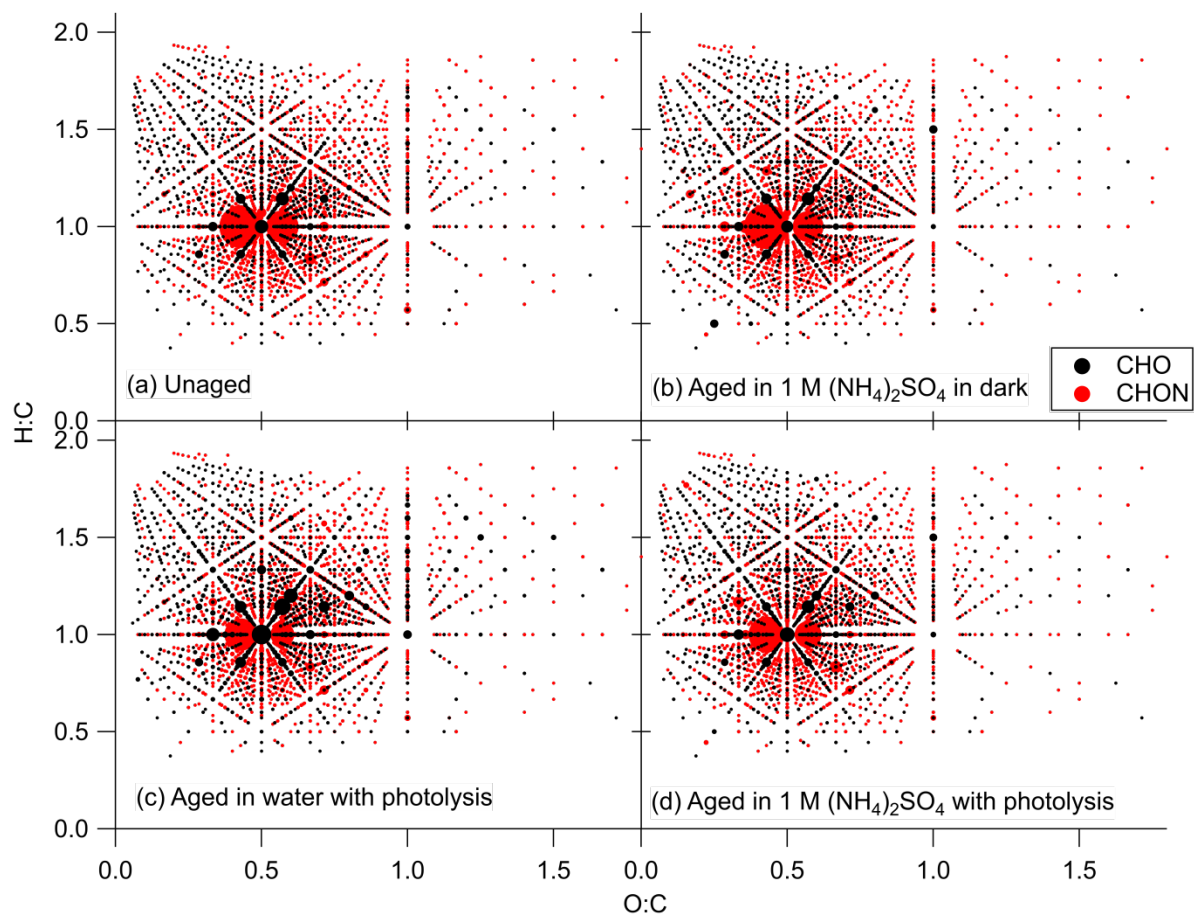
Figure S11. Van Krevelen diagrams for the (a) unaged sample, (b) sample aged in 1 M ammonium sulfate in the dark, (c) sample photolyzed in water, and (d) sample photolyzed in 1 M ammonium sulfate from Filter 4. CHO formulas are shown in black and CHON formulas are shown in red. The size of the marker represents the summed mass spectrometry abundance of all CHO or CHON compounds with the corresponding H:C and O:C ratios.

ATR-FTIR Results

Figure S12 shows the evolution of the FTIR spectra of the toluene SOA during on-filter photolysis. The aqueous conditions were too dilute for FTIR analysis, so they are not included in this method. Absorbance values are normalized to the peak intensity at 1717 cm^{-1}, which represents the carbonyl group stretching vibration. We expect carbonyl groups belonging to ketone and aldehyde functionalities to be removed through Norrish-I type reactions with photolysis (Mang et al., 2008; Lignell et al., 2013). Peaks that decrease in this plot, therefore, photolyze more readily than carbonyl compounds. Peaks corresponding to nitroaromatics (Ar-NO$_2$) and organonitrates (RONO$_2$) are denoted in the figure (Roberts, 1990; Day et al., 2010; Liu et al., 2012). It can be observed that the peaks at 1643, 1275, and 850 cm^{-1} corresponding to organonitrates decrease relative to the carbonyl peak over time. Peaks at 1556, 1539, 1360, and 1337 cm^{-1} corresponding to nitroaromatics also decrease relative to the carbonyl peak, although they do so less efficiently than the organonitrate peaks. This suggests the nitroaromatic compounds may photolyze at a slower rate than organonitrate compounds. These experiments were carried out at WM using a different lamp, so the timescales are not directly comparable with the kinetic measurements. Overall, the FTIR results show that nitrogen-containing compounds are removed during photolysis of the filters in the organic condensed phase, consistent with the HRMS results.
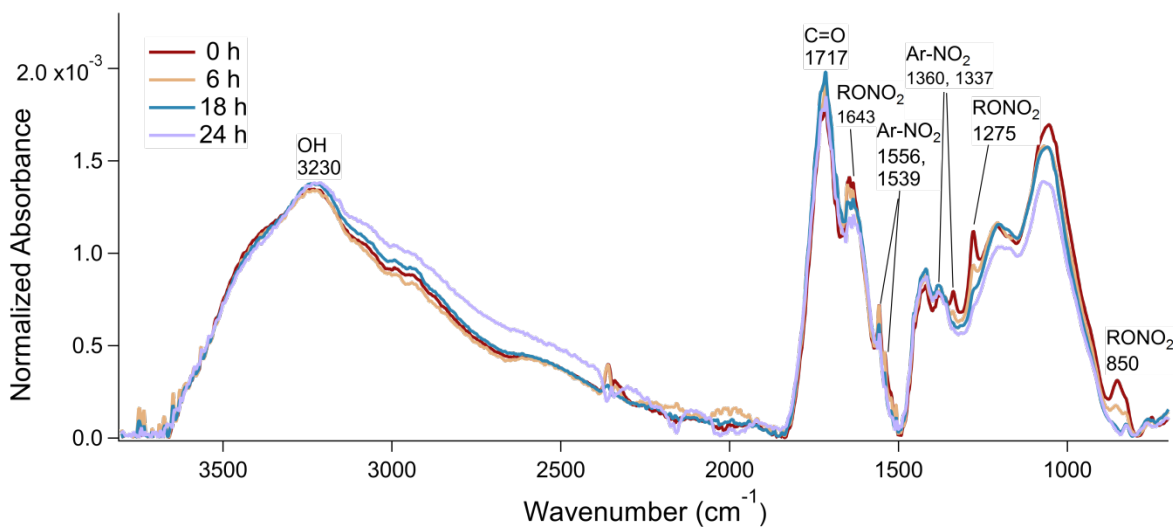
Figure S12. ATR-FTIR spectra taken after different times of on-filter photolysis normalized to the highest peak in each spectrum – the C=O peak at 1717 cm^{-1} from Filter 2. The trace for before photolysis is shown in dark red, after 6 h of photolysis in yellow, after 18 h in teal, and after 24 h in light blue. The photolysis for this experiment was performed with the irradiation set up at WM.

References

ACOM: Quick TUV: http://cprm.acom.ucar.edu/Models/TUV/Interactive_TUV/, last access: 11 July 2019.

Calvert, J., Atkinson, R., Becker, K., Kamens, R., Seinfeld, J., Wallington, T., and Yarwood, G.: The Mechanisms of Atmospheric Oxidation of Aromatic Hydrocarbons, Oxford University Press, New York, 556 pp., 2002.

Day, D. A., Liu, S., Russell, L. M., and Ziemann, P. J.: Organonitrate group concentrations in submicron particles with high nitrate and organic fractions in coastal southern California, Atmos. Environ., 44, 1970–1979, https://doi.org/10.1016/J.ATMOSENV.2010.02.045, 2010.

Klodt, A. L.: Experiment Set: Toluene SOA Generation for matrix effects study, ICARUS [data set], available at: https://icarus.ucdavis.edu/experimentset/247 (last accessed 2022-05-27), 2022.

Lignell, H., Epstein, S. A., Marvin, M. R., Shemesh, D., Gerber, B., and Nizkorodov, S.: Experimental and theoretical study of aqueous cis-pinonic acid photolysis, J. Phys. Chem. A, 117, 12930–12945, https://doi.org/10.1021/jp4093018, 2013.

Liu, S., Shilling, J. E., Song, C., Hiranuma, N., Zaveri, R. A., and Russell, L. M.: Hydrolysis of organonitrate functional groups in aerosol particles, Aerosol Sci. Technol., 46, 1359–1369, https://doi.org/10.1080/02786826.2012.716175, 2012.

Mang, S. A., Henricksen, D. K., Bateman, A. P., Andersen, M. P. S., Blake, D. R., and Nizkorodov, S. A.: Contribution of carbonyl photochemistry to aging of atmospheric secondary organic aerosol, J. Phys. Chemsitry A, 8337–8344, https://doi.org/10.1021/jp804376c, 2008.

Roberts, J. M.: The atmospheric chemistry of organic nitrates, Atmos. Environ. Part A. Gen. Top., 24, 243–287, https://doi.org/10.1016/0960-1686(90)90108-Y, 1990.

Walhout, E. Q., Yu, H., Thrasher, C., Shusterman, J. M., and O'Brien, R. E.: Effects of photolysis on the chemical and optical properties of secondary organic material over extended time scales, ACS Earth Sp. Chem., 3, 1226–1236, https://doi.org/10.1021/acsearthspacechem.9b00109, 2019.